AUTOMATED ADAPTIVE ERROR CONTROL IN FINITE ELEMENT METHODS USING THE ERROR REPRESENTATION AS ERROR INDICATOR

JOHAN JANSSON, JOHAN HOFFMAN, CEM DEGIRMENCI, JEANNETTE SPÜHLER

Abstract. In this paper we present a new adaptive finite element method directly using the a posteriori error representation as a local error indicator, and representing the primal and dual solutions in the same finite element space (here piecewise continuous linear functions on the same mesh). Since this approach gives a global a posteriori error estimate that is zero (due to Galerkin orthogonality), the error representation has traditionally been thought to contain no information about the error. However, we show the opposite, that locally, the orthogonal error representation behaves very similar to the non-orthogonal error representation using a higher order approximation of the dual, which is a standard approach to overcome the problem of a zero error estimate. We present evidence of this both in the form of an a priori estimate for the local error indicator for an elliptic model problem and a detailed computational investigation showing that the two methods exhibit very similar behavior and performance, and thus confirming the theoretical prediction. We also present computational results using a stabilized version of the method for non-elliptic partial differential equations where the error representation is no longer orthogonal, and where both the local error indicator and global error estimate behave similar to the error representation using a higher order approximation of the dual. The benefits of this adaptive method are generality and simplicity in formulation, sharpness, and efficiency since high order approximation of the dual and computation of additional constructs such as jump terms over interior facets or local problems are avoided.

1. Introduction. The setting of this paper is adaptive error control in the finite element method (FEM), which is a methodology for satisfying a tolerance on the global discretization error measured in a quantity of interest (drag/lift on an object immersed in fluid flow, displacement of a point in an elastic body, etc.) by determining how the cells in the mesh contribute to the global error and iteratively refining the approximation in those cells which have the largest contribution (or generating a new mesh to satisfy the tolerance). The a posteriori error control gives crucial *reliability* of the method since a bound on the discretization error is given, and *efficiency* since a mesh that in some sense is optimal for a given tolerance can be constructed. An a posteriori error estimate typically bounds the error in terms of a residual, mesh size, and other computable quantities. The estimate can then be split into a sum of contributions from each cell in the mesh, so-called *error indicators* where the cells with the largest contributions are marked for refinement. FEM is based on Galerkin's method, where a solution is sought for which the residual is orthogonal to all test functions in a test space. By duality the error in a functional of the FEM solution can be represented as a duality pairing of the residual and the solution of a dual problem. Typically, the dual solution needs to be approximated by computation, and if the same Galerkin FEM method is used for the dual problem, the resulting a posteriori error representation is zero due to Galerkin orthogonality. The standard approach to overcome this problem to construct adaptive methods is to use mathematical tools from functional analysis and approximation theory to derive specific a posteriori error estimates for each partial differential equation (PDE) by using integration by parts, Cauchy-Schwartz inequality and interpolation estimates, or alternatively to represent the dual and primal in different finite element spaces and use the error representation directly since it is then non-orthogonal. In this paper we present a new adaptive finite element method which is based on direct application of the a posteriori error representation as a local error indicator, and representing the primal and dual solutions in the same finite element space (here piecewise continuous linear functions on the same

mesh). Since this approach gives a global a posteriori error estimate that is zero, the error representation has traditionally been thought to contain no information about the error. However, we show the opposite, that locally, the orthogonal error representation behaves very similar to the non-orthogonal error representation using a higher order (quadratic) approximation of the dual. We present evidence of this both in the form of an a priori estimate for the local error indicator for an elliptic model problem, and a detailed computational investigation showing that the two methods exhibit very similar behavior and performance, and thus confirming the theoretical prediction. We also present a stabilized version of the method for non-elliptic PDE where the error representation is no longer orthogonal, and where both the local error indicator and global error estimate behave similar to the error representation using a higher order (quadratic) approximation of the dual. We argue, based on the evidence we present in this paper, that the method has the following advantages:

Generality and simplicity

There is no need for manual analytical derivation and computer implementation of error estimates specific to each equation or equation class, since error indicators take a generic form. The error analysis is thus much simpler, minimal in a sense, which can make it more easily accessible, widespread and suitable for automation. For a linear stationary boundary value problem formulated in a weak form with a bilinear form $a(.,.)$ and a linear form $L(.)$, a solution $u \in V$ satisfies

$$r(u,v) \equiv a(u,v) - L(v) = 0, \tag{1.1}$$

for all test functions v in the Hilbert space V, with $r(u,v)$ the weak residual, and we seek a FEM approximation $U \in V_h$ such that

$$r(U,v) = 0, \quad \forall v \in V_h. \tag{1.2}$$

In the cG(1) FEM method we let the finite element space $V_h \subset V$ consist of continuous piecewise linear functions defined on a mesh $\mathcal{T}_h$. The error indicator is then simply:

$$\mathcal{E}_K^{cG(1)} \equiv r(U,\Phi)_K, \tag{1.3}$$

where the index K indicates restriction to the cell $K \in \mathcal{T}_h$, and $\Phi \in V_h$ is the cG(1) approximation of the exact dual solution ϕ, defined by

$$a(w,\Phi) = (w,\psi), \quad \forall w \in V_h, \tag{1.4}$$

with $(.,.)$ a suitable duality pairing and ψ is the Riesz representer of the goal functional $M(\cdot) = (\cdot,\psi)$.

Reliability

For a model problem we show that the error indicator generated by the method $\mathcal{E}_K^{cG(1)} = r(U,\Phi)_K$ converges with order $1+d$ to the exact error indicator $\mathcal{E}_K = r(U,\phi)_K$:

$$\|\mathcal{E}(x) - \mathcal{E}^{cG(1)}(x)\|_{L_2(\Omega)} \leq Ch^{1+d} \tag{1.5}$$

where $\|\cdot\|_{L_2(\Omega)}$ is the L_2-norm over the domain Ω, and $\mathcal{E}(x)$ and $\mathcal{E}^{cG(1)}(x)$ are piecewise constant functions over the mesh $\mathcal{T}_h$, equal to the error indicators $\mathcal{E}_K$ and $\mathcal{E}_K^{cG(1)}$ on the cell K.
This bound indicates that the method is *reliable*, in the sense that we can control the error, which is also verified by a detailed computational study in this paper.
For a variant of the error indicator with a jump facet residual formulation of the terms with second derivatives: $\mathcal{E}_2(x)$, we prove the optimal order:

$$\|\mathcal{E}_2(x) - \mathcal{E}_2{}^{cG(1)}(x)\|_{L_2(\Omega)} \leq Ch^{2+d} \tag{1.6}$$

Efficiency

The adaptive algorithm does not require the computation of additional constructs such as jump terms over interior faces/edges in the mesh or the solution of local problems, typically generated as part of standard a posteriori error estimates, which can be costly and complex to compute, especially in a parallel programming model over distributed data.

In Section 2 we present standard approaches used to estimate the global error. We then describe our framework and present an analysis of the adaptive method in Section 3 and with a detailed computational study in Section 4. We conclude the paper with a summary and discussion.

2. State of the art. Following the standard framework developed in the 1990's by Eriksson & Johnson [7, 5, 6] and Becker & Rannacher [3, 1], with co-workers, for a linear PDE approximated by a Galerkin finite element method we can express the error in an output of interest or goal functional in terms of the weak residual acting on the solution of a dual (adjoint) problem ϕ:

$$M(u) - M(U) = r(U, \phi), \tag{2.1}$$

where ϕ in general is not available and thus needs to be approximated. If the same finite element space is used to compute the approximation of ϕ and U, the error representation is zero which follows from (1.2) We now describe the two main approaches used to bypass this problem.

2.1. Local analytical error bounds. Galerkin orthogonality can be used to subtract a projection of the dual solution on the finite element space, $\pi_h\phi \in V_h$. Asumming sufficient regularity, one can then apply integration by parts to reformulate the error representation in terms of the strong residual and use Cauchy-Schwarz inequality and interpolation error estimates to bound the error in terms of the local mesh size $h = h(x)$, the strong residual $R(U)$ and derivatives of the dual solution. That is, we can write:

$$|M(u) - M(U)| = |(R(U), \phi - \pi_h\phi)_{L_2(\Omega)}| = |\sum_{K\in\tau_h} (R(U), \phi - \pi_h\phi)_{L_2(K)}| \tag{2.2}$$

where u is the exact solution, U is the computed solution, M is the functional that defines the quantity of interest, $R(U)$ is the strong residual with possible interior facet contributions and ϕ is the solution of the dual problem. By Cauchy-Schwarz

inequality we can bound the error in the quantity of interest as:

$$|M(u) - M(U)| = |\sum_{K\in\mathcal{T}_h} (R(U), \phi - \pi_h\phi)_{L_2(K)}| \leq \sum_{K\in\mathcal{T}_h} \|R(U)\|_{L_2(K)}\|\phi - \pi_h\phi\|_{L_2(K)} \tag{2.3}$$

At this point one may use interpolation error estimates to derive estimates including $D^n\phi$, the derivatives of ϕ. Using the computed dual solution in the same FE space as the primal solution for approximating $\|D^n\phi\|_{L_2(K)}$ now makes sense since the mechanism generating the orthogonality has been removed.

2.2. Enhanced dual approximation. Another approach is to compute the dual solution using a FE space that is different from the space used for approximating the primal problem. This way the Galerkin orthogonality does not render the resulting global error representation to vanish. Many choices for choosing the FE space of the dual problem are possible as listed in [9], including using a FE space with higher degree of polynomials, a FE space that is using a supermesh obtained by global refinement, or refined adaptively by an a posteriori estimate of the dual problem for the same degree of polynomials or even a higher degree of polynomials if $hp-$adaptivity can be applied. These methods clearly increase the computational cost which can be avoided by computing the dual problem using the same FE space as the primal problem, but using patch-wise higher order interpolation inside (2.2) as mentioned in [2] and [12], which on the other hand increases the complexity of the algorithm.

3. Method description: representation adaptivity.

3.1. Model problem. To analyze the framework we choose a convection-diffusion-reaction model problem with α and ϵ scalar coefficients representing reaction and diffusion respectively, and β a vector coefficient representing the convective velocity. The model problem in weak form reads:

$$r(u, v) = (\alpha u, v) + (\epsilon\nabla u, \nabla v) + (\beta\cdot\nabla u, v) - (f, v) = 0, \quad \forall v \in V \tag{3.1}$$

with the standard space $V = H^1_g(\Omega)$, $\Omega \subset \mathbb{R}^2$ and g Dirichlet data on the boundary Γ. $(\cdot,\cdot) = (\cdot,\cdot)_{L_2}$ is the L_2 inner product, with $L_2 = L_2(\Omega)$ the space of square-integrable functions in Ω. Choosing $\beta = 0$ we obtain an elliptic model problem which we occasionally use below to simplify the analysis.

3.2. Stabilized finite element method. We solve the model problem with a Galerkin/least-squares (GLS) stabilized finite element method with continuous piecewise linear basis functions (cG(1)). That is we seek the FE solution $U \in V_h \subset V$, with V_h defined using a simplicial tessellation $\mathcal{T}_h$ of Ω with h the maximum edge length in cell K. The method reads: for all $v \in V_h$, find $U \in V_h$ such that

$$\begin{aligned} r_S(U, v) &= (\alpha U, v) + (\epsilon\nabla U, \nabla v) + (\beta\cdot\nabla U, v) - (f, v) \\ &\quad + \delta(\alpha U + \beta\cdot\nabla U - f, \alpha v + \beta\cdot\nabla v) \\ &= 0, \end{aligned}$$

where

$$\delta = \begin{cases} \frac{h}{|\beta|}, h \geq \epsilon \\ \frac{h^2}{|\beta|}, h < \epsilon \end{cases}$$

For the elliptic model problem with $\beta = 0$ no stabilization is needed, so we put $\delta = 0$.

3.3. A posteriori error estimation. We decompose the weak residual $r(U, v)$ into a bilinear form $a(U, v)$ and linear form $L(v)$ so that

$$r(U, v) = a(U, v) - L(v) \tag{3.2}$$
$$r_S(U_S, v) = a_S(U_S, v) - L_S(v) \tag{3.3}$$

and:

$$\begin{aligned} L(v) &= -r(0, v) \\ a(U, v) &= r(U, v) + L(v) \\ L_S(v) &= -r_S(0, v) \\ a_S(U_S, v) &= r_S(U, v) + L_S(v) \end{aligned} \tag{3.4}$$

with U_S denoting the computed solution from the stabilized formulation to emphasize that it's different from U, and with he errors e and e_S defined as:

$$e = u - U \tag{3.5}$$
$$e_S = u - U_S \tag{3.6}$$
$$\tag{3.7}$$

By linearity:

$$-r(U, v) = r(u, v) - r(U, v) = a(u, v) - L(v) - a(U, v) + L(v) = a(e, v), \quad \forall v \in V_h \tag{3.8}$$

using that $V_h \subset V$.

We also see that we can formulate the same relation when inserting the stabilized solution U_S into the non-stabilized weak residual $r(U_S, v)$:

$$-r(U_S, v) = r(u, v) - r(U_S, v) = a(u, v) - L(v) - a(U_S, v) + L(v) = a(e_S, v), \quad \forall v \in V_h \tag{3.9}$$

We are interested in bounding the error in a linear functional $M(U) = (U, \psi)$, which we refer to as the "output quantity", by a tolerance TOL:

$$|M(u) - M(U)| = |M(e)| = |(e, \psi)| < TOL \tag{3.10}$$

3.3.1. Dual problem. We introduce the dual problem with solution ϕ and a source term ψ:

$$a(w, \phi) = (w, \psi), \quad \forall w \in V \tag{3.11}$$

noting that we have switched the order of the arguments in the bilinear form $a(\cdot, \cdot)$. A discrete approximation Φ to the dual solution is computed with the same stabilized method as for the primal problem:

$$a_S(w, \Phi) = (w, \psi) \quad \forall w \in V_h, \quad \Phi \in V_h \tag{3.12}$$

3.3.2. A posteriori error estimate. We can express the error in the output quantity exactly by the residual and the dual solution:

$$M(u) - M(U) = (e, \psi) = a(e, \phi) = -r(U, \phi) \tag{3.13}$$

and similarly for the stabilized solution U_S:

$$M(u) - M(U_S) = (e_S, \psi) = a(e_S, \phi) = -r(U_S, \phi) \tag{3.14}$$

Thus an error estimate can trivially be stated as:

$$|M(u) - M(U)| = |r(U, \phi)| \tag{3.15}$$

and again for U_S:

$$|M(u) - M(U_S)| = |r(U_S, \phi)| \tag{3.16}$$

for cases where we compute a stabilized solutution U_S, we will use the error estimate (3.16) which is not orthogonal.

3.4. Standard a posteriori error estimate with projected facet terms. When deriving a standard a posteriori error estimate of a PDE with second-order differential operators, one typically uses integration by parts to generate interior facet terms, representing the second derivative in weak form. To have a mix of interior and facet integral terms in the estimate can make the analysis more difficult, requiring trace estimates and more complex notation. This section shows how to use an exact L_2-projection to represent the facet terms as volume terms, greatly simplifying the analysis and notation. From (3.15) we perform integration by parts, moving derivatives of ϕ back to U to reconstruct the strong residual $R(U)$ and generate facet terms $R_F(U)$:

$$r(U, \phi) = \sum_{K \in \mathcal{T}_h} r(U, \phi)_K = \sum_{K \in \mathcal{T}_h} (R(U), \phi)_K + (R_F(U), \phi)_{\partial K} \tag{3.17}$$

To represent $R_F(U)$ as a volume term $R_F^{dG(0)}(U)$, we formulate a standard L_2-projection onto W_h, the space of discontinuous piecewise constant basis functions ($dG(0)$):

$$\sum_{\partial K \in \mathcal{T}_h} (R_F(U), v)_{\partial K} = (R_F^{dG(0)}(U), v), \quad \forall v \in W_h \tag{3.18}$$

The estimate can now be written in the compact form:

$$|r(U, \phi)| = |(R(U) + R_F^{dG(0)}(U), \phi)| \equiv |(R_\Sigma(U), \phi)| \tag{3.19}$$

with $R_\Sigma(U)$ denoting the sum of all contributions to the residual expression.

3.4.1. Two different facet residual formulations. By choosing to associate the facet integrals with the cells K_i, $i = 1, 2$, sharing the facet in different ways, we can write different formulations of the facet residual with different convergence properties, but with the same functional value.

Facet residual formulation 1. In the first variant we can choose a facet formulation which associates only the facet integrals from the element itself, which we denote $R_{F,1}$, and we let $R_{\Sigma,1}$ denote for the whole residual:

$$(\nabla U, \nabla \phi) = \int_{\partial K} \nabla U \cdot n_{\partial K} \phi ds \tag{3.20}$$

$$R_{F,1}(U, \phi) \equiv \int_{\partial K} \nabla U \cdot n_{\partial K} \phi ds \tag{3.21}$$

this formulation is equivalent to the original weak residual $(\nabla U, \nabla \phi)$ since we only perform operations inside the cell K.

Facet residual formulation 2. In the second variant we associate half of the facet integral from the element itself and half of the facet integral from the element sharing the facet, generating a "jump", we denote this formulation $R_{F,2}$ with $R_{\Sigma,2}$ denoting for the whole residual:

$$(\nabla U, \nabla \phi) = \sum_{K \in \mathcal{T}_h} \frac{1}{2} \int_{\partial K} [\nabla U] \cdot n_{\partial K} \phi ds \tag{3.22}$$

$$R_{F,2}(U, \phi) \equiv \sum_{K \in \mathcal{T}_h} \frac{1}{2} \int_{\partial K} [\nabla U] \cdot n_{\partial K} \phi ds \tag{3.23}$$

where $[\nabla U] = \nabla U|_{K_1} - \nabla U|_{K_2}$ denotes the "jump" in the gradient ∇U across the facet shared by the cells K_1 and K_2.

3.5. Adaptive error control. We are now ready to use our a posteriori error estimate to control the error in a finite element discretization by adaptive mesh refinement. To be able to compute the error estimate, we need to compute also the dual solution by a finite element discretization. We introduce the discrete dual solution Φ and the discrete a posteriori error estimate $|r(U, \Phi)|$. Having the exact dual, our error control would be based on satisfying:

$$|M(u) - M(U)| = |r(U, \phi)| \leq TOL \tag{3.24}$$

Using the computable error estimate, the error control is instead based on satisfying:

$$|r(U, \Phi)| \leq TOL \tag{3.25}$$

3.5.1. Error indicator. To be able to decide which cells in the mesh $\mathcal{T}_h$ to refine, we write the error estimate as a sum over all cells:

$$|r(U, \Phi)| = |\sum_{K \in \mathcal{T}_h} r(U, \Phi)_K| = \sum_{K \in \mathcal{T}_h} |r(U, \Phi)_K| \tag{3.26}$$

We denote this cell-based quantity as the *error indicator* $\mathcal{E}_K^{cG(1)}$, with the $cG(1)$ superscript indicating that the dual solution is approximated using cG(1) finite elements:

$$\mathcal{E}_K \equiv r(U, \phi)_K \tag{3.27}$$

$$\mathcal{E}_K^{cG(1)} \equiv r(U, \Phi)_K \tag{3.28}$$

The error indicators can also be represented as functions in space $\mathcal{E}(x)$ and $\mathcal{E}^{cG(1)}(x)$ by expansion in piecewise discontinuous constant basis functions $\theta_K \in W_h$ ($\theta_K = 1$

in cell K, and 0 in all other cells):

$$\mathcal{E}(x) = \sum_{K\in\tau_h} \mathcal{E}_K\theta_K(x) = \sum_{K\in\tau_h} r(U,\phi)_K\theta_K(x) \tag{3.29}$$

$$\mathcal{E}^{cG(1)}(x) = \sum_{K\in\tau_h} \mathcal{E}_K^{cG(1)}\theta_K(x) = \sum_{K\in\tau_h} r(U,\Phi)_K\theta_K(x) \tag{3.30}$$

We denote $\mathcal{E}(x)$ and $\mathcal{E}^{cG(1)}(x)$ as *error indicator functions*.

3.5.2. Adaptive mesh refinement algorithm. Based on the error indicator we can form adaptive algorithms for how to construct finite element meshes optimized to control the error in the functional $M(U)$.

Starting from an initial coarse mesh $\mathcal{T}_h^0$, one such simple algorithm takes the following form: let $k = 0$ then do

ALGORITHM 1. *Adaptive mesh refinement*

1. *For the mesh $\mathcal{T}_h^k$: compute the primal problem and the dual problem.*
2. *If $|\sum_{K=1}^M \mathcal{E}_K^{cG(1)}| < TOL$ or $|M(U^k) - M(U^{k-1})| < \gamma * TOL$ then stop, else:*
3. *Mark some chosen percentage of the elements with highest $|\mathcal{E}_K^{cG(1)}|$ for refinement.*
4. *Generate the refined mesh $\mathcal{T}_h^{k+1}$ (e.g. by Rivara bisection [11]), set $k = k+1$, and goto 1.*

Here the second stopping condition $|M(U^k) - M(U^{k-1})| < \gamma * TOL$ is used for the case of an orthogonal error representation.

3.6. A priori error estimate of the error indicator. Finally, we derive an a priori estimate for the error indicator with cG(1) approximation of the dual for the elliptic model problem (the model problem (3.1) with $\beta = 0$), and show that even though the *global error estimate* is zero: $|r(U,\Phi)| = 0$, the *error indicator function* $\mathcal{E}^{cG(1)}(x)$ (and thus the error indicators it is composed of) is of good quality and converges to the exact error indicator function $\mathcal{E}(x)$ with order 1 + d or 2 + d, with d the geometric dimension, for the plain weak residual or a variant of the error indicator with a jump facet formulation for second order derivative terms. The key to this analysis is the realization that even if the error representation is zero: $|r(U,\Phi)| = 0$, the L_2-norm of the *error indicator function* is typically not: $\|\mathcal{E}^{cG(1)}(x)\|_{L_2} > 0$, unless the function itself is zero everywhere, which is not a relevant case. We divide the estimate into two cases corresponding to the two different facet residual formulations $R_{F,1}$ and $R_{F,2}$ for terms with second order derivatives. The first facet residual formulation $R_{F,1}$ is equivalent to using the weak residual without facet integrals, whereas the second facet residual formulation $R_{F,2}$ involves distributing the facet contributions between the cells K_i sharing the facet and therefore gives a different L_2 norm and different convergence in the L_2 norm.

3.6.1. Standard estimates. We recall some standard estimates which we will use for our derivation of an a priori estimate, where C_i denotes an interpolation constant. A basic estimate of the L_2-projection Pf of a function f onto the space W_h:

$$\|Pf\|_{L_2} \leq \|f\|_{L_2} \tag{3.31}$$

The standard interpolation estimates for piecewise linear (cG(1)):

$$\|f - \pi^{cG(1)}f\|_{L_2} \leq C_i h^2 \|D^2 f\|_{L_2} \tag{3.32}$$

and quadratic (cG(2)) polynomials:

$$\|f - \pi^{cG(2)} f\|_{L_2} \leq C_i h^3 \|D^3 f\|_{L_2}, \tag{3.33}$$

where h denotes the maximum element size. For the case of the elliptic model problem one can show the following a priori and a posteriori estimates for $\Phi \in \text{cG}(1)$ in the L_2 norm, see e.g. [6, 4]:

$$\|\phi - \Phi\|_{L_2} \leq C_i h^2 \|D^2 \phi\|_{L_2} \tag{3.34}$$

$$\|\phi - \Phi\|_{L_2} \leq C_i h^2 \|R_\Sigma(\Phi)\|_{L_2} \tag{3.35}$$

Using these estimates and assuming that $\epsilon, \alpha \in H^1(\Omega)$ are positive and $u \in H^2(\Omega)$, we see that the second facet residual formulation must be bounded by a constant C_R independent of h, for a detailed proof see [8].

$$\|R_{\Sigma,2}(U)\|_{L_2} \leq C_{R_2} \tag{3.36}$$

For the first facet residual formulation we give experimental numerical evidence in figure 4.3 that the convergence behaves like:

$$\|R_{\Sigma,1}(U)\|_{L_2} \leq C_{R_1} h^{-1} \tag{3.37}$$

3.6.2. Derivation of the a priori estimate. We begin by re-arranging our error indicator expressions:

$$\begin{aligned} \mathcal{E}(x) - \mathcal{E}^{cG(1)}(x) &= \sum_{K \in \tau_h} r(U, \phi)_K \theta_K(x) - \sum_{K \in \tau_h} r(U, \Phi)_K \theta_K(x) \\ &= \sum_{K \in \tau_h} r(U, \phi - \Phi)_K \theta_K(x) \end{aligned} \tag{3.38}$$

We then use the projected form of the facet terms in the residual (see eq. (3.19)) to separate out the error in the dual solution ϕ:

$$\sum_{K \in \tau_h} r(U, \phi - \Phi)_K \theta_K(x) = \sum_{K \in \tau_h} (R_\Sigma(U), \phi - \Phi)_K \theta_K(x) \tag{3.39}$$

We consider two different facet formulations $R_{\Sigma,1}(U)$ and $R_{\Sigma,2}(U)$, and since the second formulation affects the L_2 norm by distributing the facet integrals between cells, we keep the error indicators apart by the corresponding subscript below. We now continue to analyze the convergence in the L_2 norm:

$$\| \sum_{K \in \tau_h} (R_\Sigma(U), \phi - \Phi)_K \theta_K(x) \|_{L_2} \tag{3.40}$$

We note that the L_2-projection Pf of a function f onto the space of piecewise constants W_h can be written as:

$$Pf(x) = \sum_{K \in \tau_h} \frac{1}{|K|} \int_K f dx \theta_K(x) \tag{3.41}$$

Writing out the inner product as an integral, we thus see that we have the L_2-projection of the integrand $R_\Sigma(U)(\phi - \Phi)$ onto the space of piecewise constants W_h weighted by the cell volume $|K|$:

$$\| \sum_{K \in \tau_h} \int_K R_\Sigma(U)(\phi - \Phi) dx \theta_K(x) \|_{L_2} = \| |K| P(R_\Sigma(U)(\phi - \Phi)) \|_{L_2} \tag{3.42}$$

Using (3.31) and $|K| \leq C_K h^d$ with d the geometric dimension gives:

$$\| |K| P(R_\Sigma(U)(\phi - \Phi)) \|_{L_2} \leq C_K h^d \| R_\Sigma(U)(\phi - \Phi) \|_{L_2} \tag{3.43}$$

Continuing with Cauchy-Schwartz and (3.34) we get:

$$\begin{aligned} C_K h^d \| R_\Sigma(U)(\phi - \Phi) \|_{L_2} &\leq C_K h^d \| R_\Sigma(U) \|_{L_2} \| \phi - \Phi \|_{L_2} \\ &\leq C_K h^d C_i h^2 \| D^2 \phi \|_{L_2} \| R_\Sigma(U) \|_{L_2} \end{aligned} \tag{3.44}$$

Using (3.36) and defining the constant C we can write:

$$C_i C_K \| D^2 \phi \|_{L_2} \| R_\Sigma(U) \|_{L_2} \leq C \tag{3.45}$$

For the second facet formulation $R_{\Sigma,2}$ we have the sought-after a priori estimate for the cG(1) error indicator ${\mathcal{E}_2}^{cG(1)}(x)$, where we indicate the choice of facet formulation by a subscript:

$$\| \mathcal{E}_2(x) - {\mathcal{E}_2}^{cG(1)}(x) \|_{L_2} \leq C h^{2+d} \tag{3.46}$$

For the first facet formulation $R_{\Sigma,1}$, which is also equivalent to the weak residual, we have based on numerical experimental evidence for the convergence of the residual, again indicating the choice of facet residual formulation by a subscript:

$$\| \mathcal{E}_1(x) - {\mathcal{E}_1}^{cG(1)}(x) \|_{L_2} \leq C h^{1+d} \tag{3.47}$$

We also state a variant of the estimates comparing against a piecewise quadratic dual $\Phi^{cG(2)}$ instead of the exact dual ϕ:

$$\| {\mathcal{E}_2}^{cG(2)}(x) - {\mathcal{E}_2}^{cG(1)}(x) \|_{L_2} \leq C h^{2+d} \tag{3.48}$$

$$\| {\mathcal{E}_1}^{cG(2)}(x) - {\mathcal{E}_1}^{cG(1)}(x) \|_{L_2} \leq C h^{1+d} \tag{3.49}$$

3.7. Error indicator effectivity index. Traditionally, the performance of an a posteriori error estimate and its corresponding error indicator are measured by the *effectivity index* I_{eff}:

$$I_{eff} = \frac{|r(U, \Phi)|}{|(e, \psi)|} \tag{3.50}$$

where we expect the index to be 1 for an optimal error estimate.

However, in the case of an orthogonal error representation we see that the index is 0, which would appear to indicate that the error indicator has zero effectivity and performance. In the previous section we derived an a priori estimate showing that the local error indicator of the orthogonal cG(1) error representation is very close to the non-orthogonal cG(2) error representation (also shown in the computational study below). This appears contradict the statement that the error indicator has zero

effectivity and performance, and motivates an extension of the effectivity concept. To be able to analyze adaptive methods in this setting we introduce an additional effectivity index of the *error indicator* rather than of the *error estimate*. The *error indicator effectivity index* I_{eieff} of the $\mathcal{E}^{cG(1)}(x)$ error indicator is defined as:

$$I_{eieff} = \frac{\|\mathcal{E}^{cG(1)}(x) - \mathcal{E}(x)\|_{L_2}}{\|\mathcal{E}(x)\|_{L_2}} \tag{3.51}$$

with $\mathcal{E}(x)$ the error indicator resulting from using the exact dual solution ϕ. To achieve a computable error indicator effectivity index, we define the *cG(2) error indicator effectivity index* where we instead use $\mathcal{E}^{cG(2)}(x)$ as the reference error indicator, i.e. using a quadratic approximation of the dual:

$$I_{eieff}^{cG(2)} = \frac{\|\mathcal{E}^{cG(1)}(x) - \mathcal{E}^{cG(2)}(x)\|_{L_2}}{\|\mathcal{E}^{cG(2)}(x)\|_{L_2}} \tag{3.52}$$

I_{eieff} measures the quality of the local error indicator against the local error indicator generated from the exact error representation, which is an error estimate that is equal to the error and has effectivity index 1. $I_{eieff}^{cG(2)}$ similarly measures against the local error indicator and error estimate with a cG(2) dual, which is considered as an excellent error estimate [8], but too expensive for real applications, since it costs as much as solving the primal problem with a higher order polynomial approximation, i.e. a uniform p-refinement. We therefore use the cG(2) dual as a computable reference in a test setting.

4. Computational results. We present a detailed computational study comparing the $cG(1)$ representation adaptivity method ("rep") against the $cG(2)$ representation adaptivity method ("quad"), a standard Cauchy-Schwartz based adaptive method with projected jump terms and first order interpolation ("jump"), second order interpolation ("jump2") and uniform mesh refinement ("uniform"). For the adaptive methods we refine 10% of the marked cells in each adaptive iteration.

We use the "jump2" solution on the finest mesh as the reference solution, since the method is standard, robust and well-proven (see e.g. [6]).

4.1. Specific problem statement. We repeat the model problem formulation (3.1) from above :

$$r(u,v) = (\alpha u, v) + (\epsilon \nabla u, \nabla v) + (\beta \cdot \nabla u, v) - (f, v) = 0, \quad \forall v \in V$$

with the standard space $V = H_g^1(\Omega)$, $\Omega \subset R^2$ and g data on the boundary Γ. The domain is chosen to be a square with a hole in the center:

$$\Omega = (0,0) \times (1,1) \setminus (0.48, 0.48) \times (0.52, 0.52) \tag{4.1}$$

The data g is chosen to be $g = 0$ on the outer boundary and $g = 10$ on the inner hole boundary.

The convective velocity β is constant and chosen so as not to be aligned with the cells in a uniform mesh:

$$\beta = (-1, -0.61) \tag{4.2}$$

The other coefficients in the equation are varied to generate a range of test problems, and are stated in the test problem list below.

The output functional is chosen as a Gaussian function concentrated in the lower-left quadrant:

$$\psi = e^{(-20|x-(0.25,0.25)|^2)} \tag{4.3}$$

We choose ψ smooth to avoid special treatment of possible discontinuities and set the source term to zero, $f = 0$. The geometry and a sample solution is shown in figure 4.1.

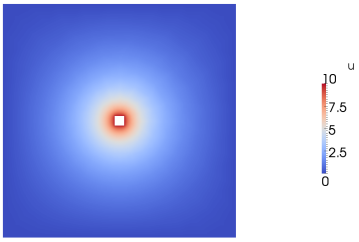

FIG. 4.1. *The geometry and sample solution for the test problems.*

4.2. Test problems. We use the model problem in (3.1) and consider three sets of parameters:

Elliptic $\alpha = 1, \epsilon = 10^{-1}, \beta = 0$, an elliptic test problem where the error representation is orthogonal for the "rep" method. The graphs of convergence and performance indices are plotted in figure 6.1. The primal and dual solution and mesh are plotted in figure 6.2, and the error indicator for adaptive iteration 0 and 10 are plotted in figure 6.7

Diffusion-dominated $\alpha = 1, \epsilon = 10^{-1}, |\beta| = 1.171$, a diffusion-dominated test problem where the error representation is non-orthogonal due to stabilization for the "rep" method. The graphs of convergence and performance indices are plotted in figure 6.3. The primal and dual solution and mesh are plotted in figure 6.4, and the error indicator for adaptive iteration 0 and 10 are plotted in figure 6.8

By choosing a more refined initial mesh, one could with reasonable cost avoid having to stabilize the method. With the initial mesh we have here however, stabilization is required, and this setting thus tests the situation where both cases of the δ stabilization coefficient are used.

Convection-dominated $\alpha = 1, \epsilon = 10^{-5}, |\beta| = 1.171$, a convection-dominated test problem where the error representation is non-orthogonal for the "rep" method due to stabilization. The graphs of convergence and performance indices are plotted in figure 6.5. The solution, dual and mesh are plotted in figure 6.6, and the error indicator for adaptive iteration 0 and 10 are plotted in figure 6.9

4.3. Order verification for the a priori estimate. To verify the order predicted by the a priori estimate we uniformly refine the mesh for the test problem above and compute $log_2(\frac{\|\mathcal{E}^{cG(2),k}(x)-\mathcal{E}^{cG(1),k}(x)\|_{L_2}}{\|\mathcal{E}^{cG(2),k+1}(x)-\mathcal{E}^{cG(1),k+1}(x)\|_{L_2}})$ with k and $k+1$ two consecutive adaptively refined meshes. Since the test problem is non-smooth (the corners of the center hole give singularities in the solution), we also introduce a smooth variant of the test problem and perform the above order verification for both problems in

table 4.2. We expect the order for the smooth problem to be 3 for $R_{J,1}$ (which we strongly verify) and 4 for $R_{J,2}$. The order for the non-smooth problem is reduced and our results seem to give an order of ca. 2.3.

The smooth variant of the elliptic test problem ($\alpha = 1, \epsilon = 10^{-1}, \beta = 0$) without the center hole reads:

$$\Omega = (0,0) \times (1,1) \tag{4.4}$$

The output functional is chosen as a linear function for simplicity:

$$\psi = x_0 + x_1 \tag{4.5}$$

And the source term is chosen as unity: $f = 1$ to drive the problem.

5. Discussion and conclusion. In this paper we have investigated an adaptive finite element method where we directly use the error representation as error indicator, and compute the dual solution in the same space as the primal (both cG(1)). We denote the method "cG(1) representation adaptivity" since we directly use the cG(1) error representation as error indicator. This approach has historically been discarded a priori since the error representation is orthogonal and equal to zero, and thus has been thought to contain no information. We have shown the opposite by an a priori estimate of the error indicator and a detailed computational study, showing that the error indicator defined by the orthogonal error representation is very close to the error indicator defined by the non-orthogonal error representation using a quadratic approximation of the dual.

Refinement level	Order for non-smooth test problem $R_{J,1}$	Order for non-smooth test problem $R_{J,2}$	Order for smooth test problem $R_{J,1}$	Order for smooth test problem $R_{J,2}$
1	2.83	2.89	3.01	3.93
2	2.76	2.56	3.00	3.97
3	2.61	2.41	3.00	3.99
4	2.48	2.36	3.00	3.99
5	2.40	2.34	3.00	4.00

FIG. 4.2. *Computational verification of convergence order of cG(1) error indicator with regard to the cG(2) error indicator. We compute* $log_2(\frac{\|\mathcal{E}^{cG(2),k}(x) - \mathcal{E}^{cG(1),k}(x)\|_{L_2}}{\|\mathcal{E}^{cG(2),k+1}(x) - \mathcal{E}^{cG(1),k+1}(x)\|_{L_2}})$ *with* k *and* $k+1$ *indicating the refinement level, which gives the convergence order under uniform refinement (the mesh size* h *is halved each refinement level).*

Refinement level	Order for $R_{F,1}(U)$	Order for $R_{F,2}(U)$
1	-1.02	-0.05
2	-1.02	-0.03
3	-1.01	-0.01
4	-1.00	-0.01
5	-1.00	-0.00

FIG. 4.3. *Computational verification of convergence order of the two facet residual variants. We compute* $log_2(\frac{\|R^k_{F,\cdot}(U)\|_{L_2}}{\|R^{k+1}_{F,\cdot}(U)\|_{L_2}})$ *with* k *and* $k+1$ *indicating the refinement level, which gives the convergence order under uniform refinement (the mesh size* h *is halved each refinement level).*

For extension to non-linear and convection-dominated problems such as Navier-Stokes equations, see [10].

Specific conclusions we can derive from the results are:

Convergence of the cG(1) error indicator The cG(1) orthogonal error indicator converges to the exact error indicator (with exact dual) with order $1 + d$ for the weak residual formulation and with order $2 + d$ for a jump facet residual formulation for terms with second order derivatives. We prove this in the a priori estimates (3.46) and (3.47), and computationally verify the prediction in table 4.2.

Similar behavior between the cG(1) and cG(2) error indicators The detailed computational study presented in figures 6.1-6.9 shows that the plots of the adaptively generated meshes, error and error estimates are very similar, a close visual inspection is needed to see differences in the meshes for example.

Good quality error estimate of the cG(1) error indicator with stabilization Using the cG(1) error indicator for a stabilized method no longer gives an orthogonal error representation and indicator. Since we have shown that the error indicator is of very good quality (aside from the orthogonality making the estimate 0) in the a priori estimate for elliptic problems, we expect the error estimate in the stabilized case to also be of good quality. In figures 6.3 and 6.9 we can verify that this is the case, with the error estimate outperforming the Cauchy-Schwarz jump estimates by up to an order of magnitude, except in one point where the quality of the reference solution may cause an abberation.

Similar performance of the error indicators In figures 6.1, 6.3 and 6.9 we see that the *error* for all the adaptive methods behave similarly, specifically the cG(1)/cG(2) and "jump"/"jump2" error indicators, except for the convection-dominated test case, where the Cauchy-Schwarz "jump"-type methods give a significantly lower error than the representation-type methods. This is something we would like to investigate in the future.

Good quality error indicator efficiency index for the cG(1) error indicator We plot the cG(2) error indicator efficiency index $I_{eieff}^{cG(2)}$ for the cG(1) error indicator for all test cases in figures 6.1, 6.3 and 6.9, which gives an indication of the efficiency of the cG(1) error indicator compared to the cG(2) error indicator. We see that the indicator is below 10% for the elliptic and diffusion-dominated test problems, and decrease as we refine the mesh, and below 50% for the convection-dominated test case for the coarse meshes, and decreasing to below 10% for the finer meshes.

Adaptive methods outperforming uniform refinement Lastly, we see that for all test problems (even the elliptic test problem), the adaptive methods outperform uniform refinement, by up to 3 orders of magnitude in the error.

6. Acknowledgements. This research has been supported by EU-FET grant EUNISON 308874, the European Research Council, the Swedish Foundation for Strategic Research, the Swedish Research Council and the Basque Excellence Research Center (BERC) program by the Basque Government.

REFERENCES

[1] Roland Becker and Rolf Rannacher. A feed-back approach to error control in adaptive finite

element methods: Basic analysis and examples. *East-West J. Numer. Math.*, 4:237–264, 1996.

[2] Roland Becker and Rolf Rannacher. An optimal control approach to a posteriori error estimation in finite element methods. *Acta Numerica*, 10:1–102, 5 2001.

[3] Roland Becker and Rolf Rannacher. A posteriori error estimation in finite element methods. *Acta Numer.*, 10:1–103, 2001.

[4] M Crouzeix and V Thomée. The stability in l_p and w_pˆ1 of the l_2-projection onto finite element function spaces. *Mathematics of Computation*, pages 521–532, 1987.

[5] Kenneth Eriksson, Don Estep, Peter Hansbo, and Claes Johnson. Introduction to adaptive methods for differential equations. *Acta Numer.*, 4:105–158, 1995.

[6] Kenneth Eriksson, Don Estep, Peter Hansbo, and Claes Johnson. *Computational Differential Equations*. Cambridge University Press New York, 1996.

[7] Kenneth Eriksson and Claes Johnson. An adaptive finite element method for linear elliptic problems. *Math. Comp.*, 50:361–383, 1988.

[8] Donald Estep. A short course on duality, adjoint operators, greens functions, and a posteriori error analysis. *Lecture Notes*, 2004.

[9] Michael B. Giles and Endre Sli. Adjoint methods for pdes: a posteriori error analysis and postprocessing by duality. *Acta Numerica*, 11:145–236, 1 2002.

[10] Johan Jansson, Jeannette Spũhler, Cem Degirmenci, and Johan Hoffman. Automated error control in finite element methods with applications in fluid flow. *Technical Report KTH-CTL, Computational Technology Laboratory*, 2014.

[11] M-C. Rivara. Local modification of meshes for adaptive and/or multigrid finite-element methods. *Journal of Computational and Applied Mathematics*, 36(1):78–89, 1992.

[12] Marie E Rognes and Anders Logg. Automated goal-oriented error control i: Stationary variational problems. *SIAM Journal on Scientific Computing*, 35(3):C173–C193, 2013.

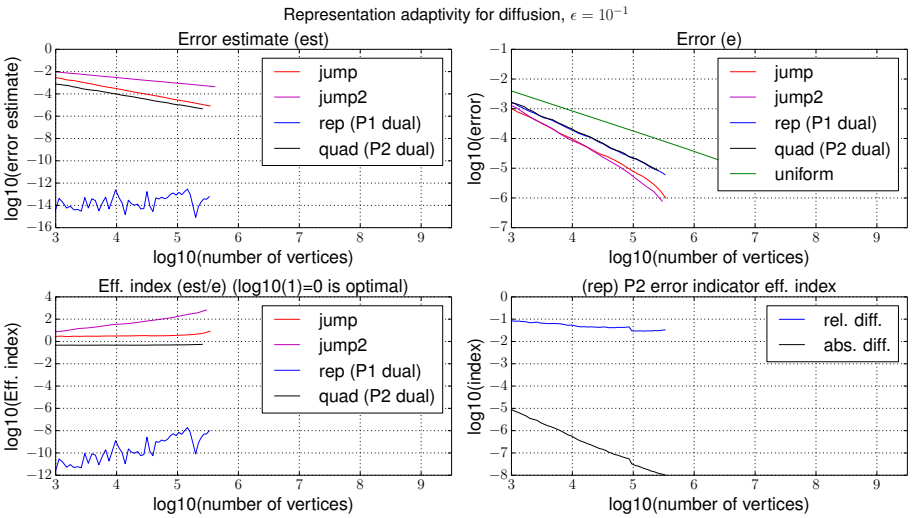

FIG. 6.1. *Graphs of error control quantities for the test problem (annoted in the graphs).*

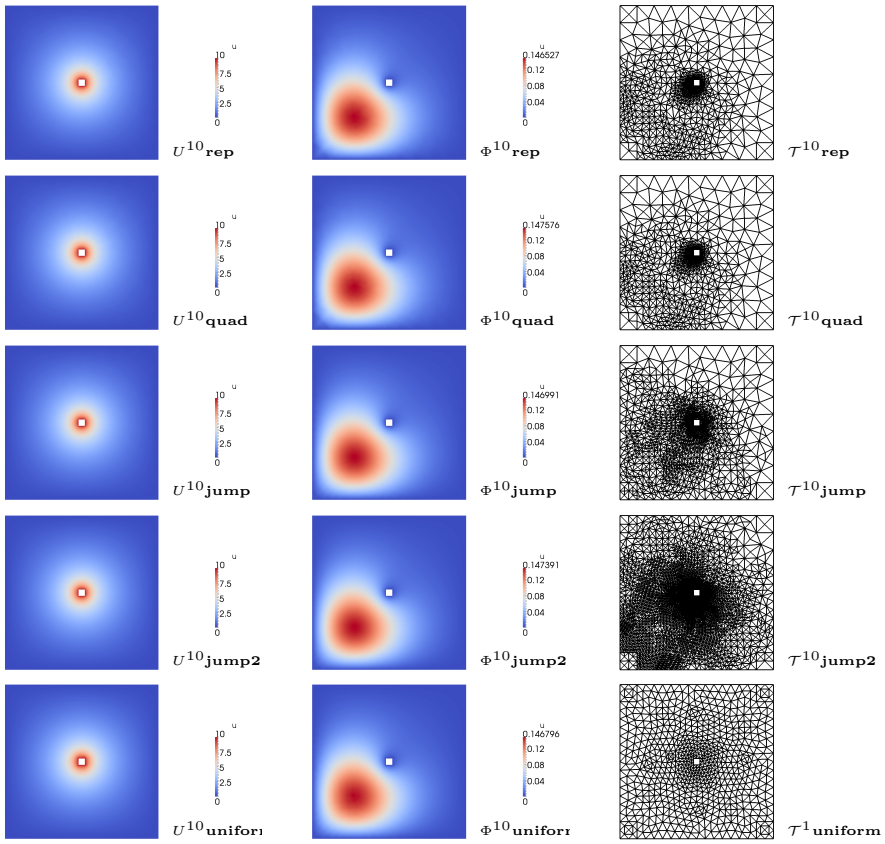

FIG. 6.2. *Comparison of solution U and dual Φ for all methods for $\epsilon = 10^{-1}, |\beta| = 0$*

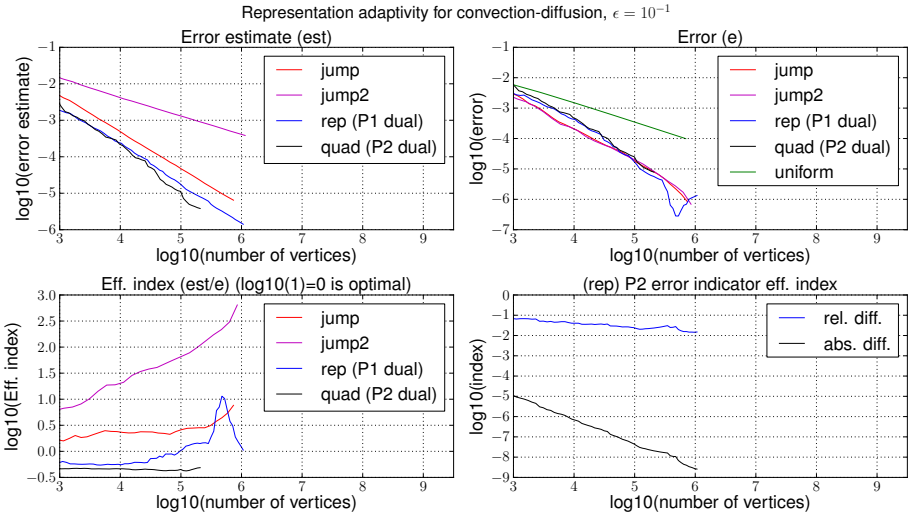

FIG. 6.3. *Graphs of error control quantities for the test problem (annoted in the graphs).*

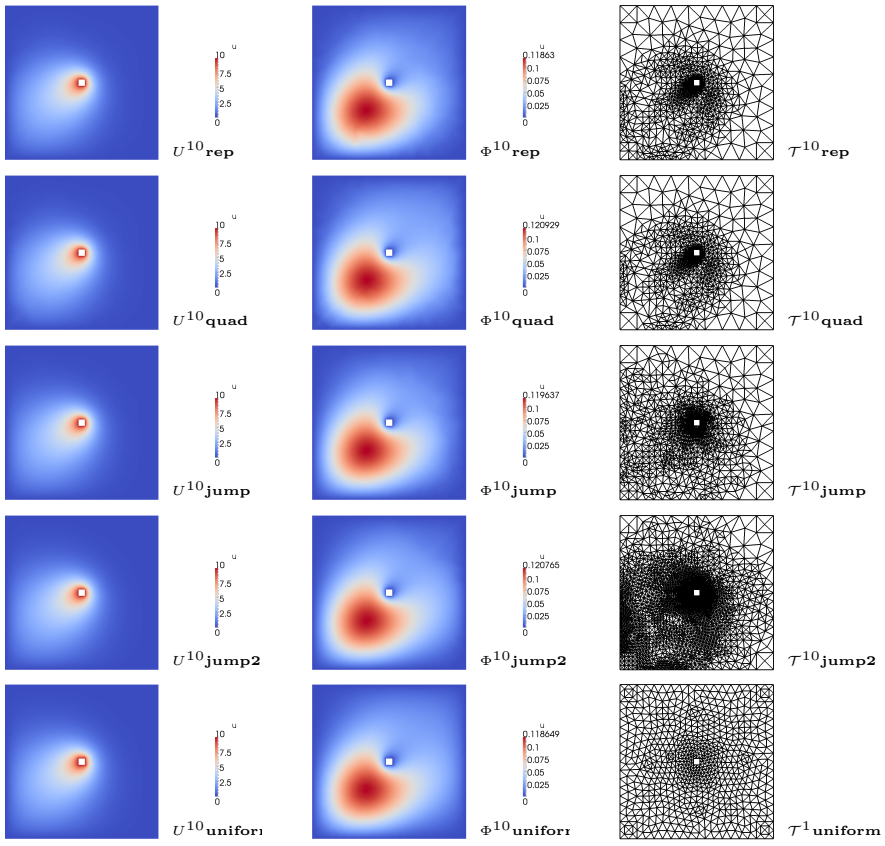

FIG. 6.4. *Comparison of solution U and dual Φ for all methods for $\epsilon = 10^{-1}, |\beta| = 1.171$*

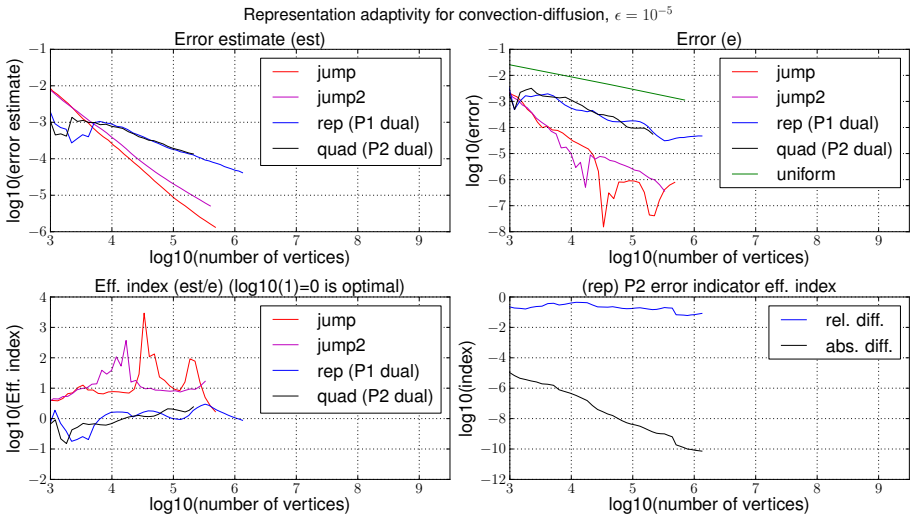

FIG. 6.5. *Graphs of error control quantities for the test problem (annoted in the graphs).*

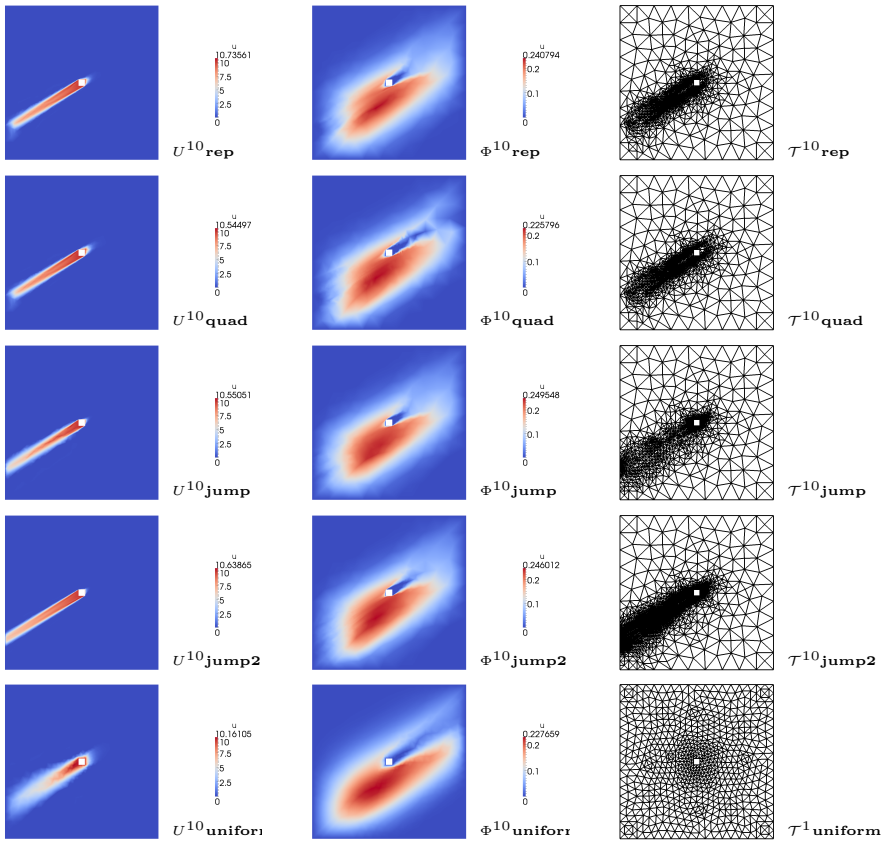

FIG. 6.6. *Comparison of solution U and dual Φ for all methods for $\epsilon = 10^{-1}, |\beta| = 1.171$*

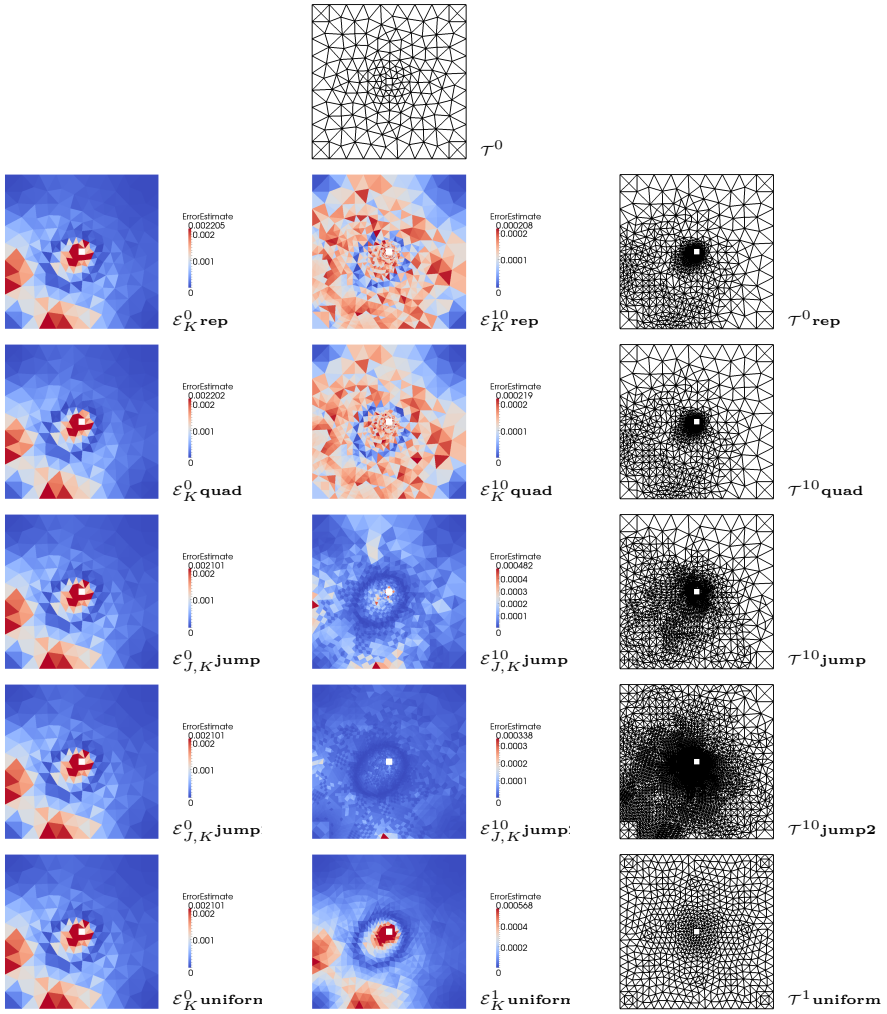

FIG. 6.7. *Comparison of adaptive error control quantitites and meshes for all methods for* $\epsilon = 10^{-1}, |\beta| = 0$

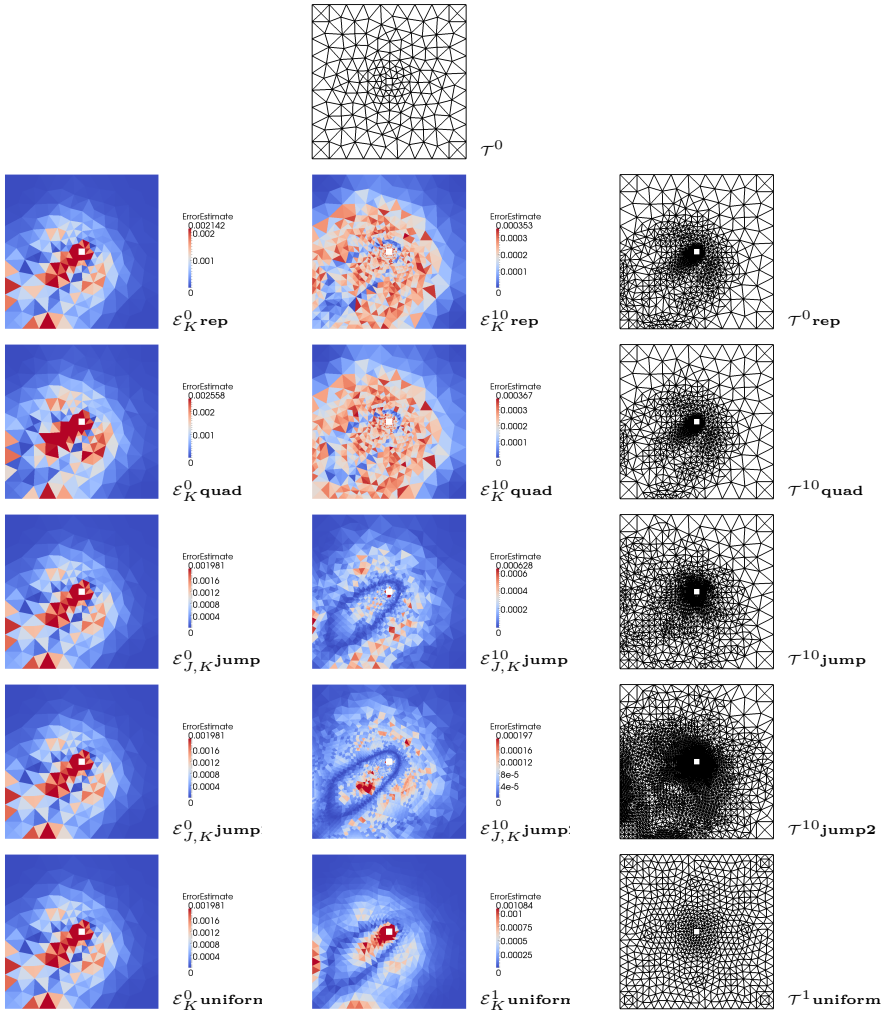

FIG. 6.8. *Comparison of adaptive error control quantitites and meshes for all methods for* $\epsilon = 10^{-1}, |\beta| = 1.171$

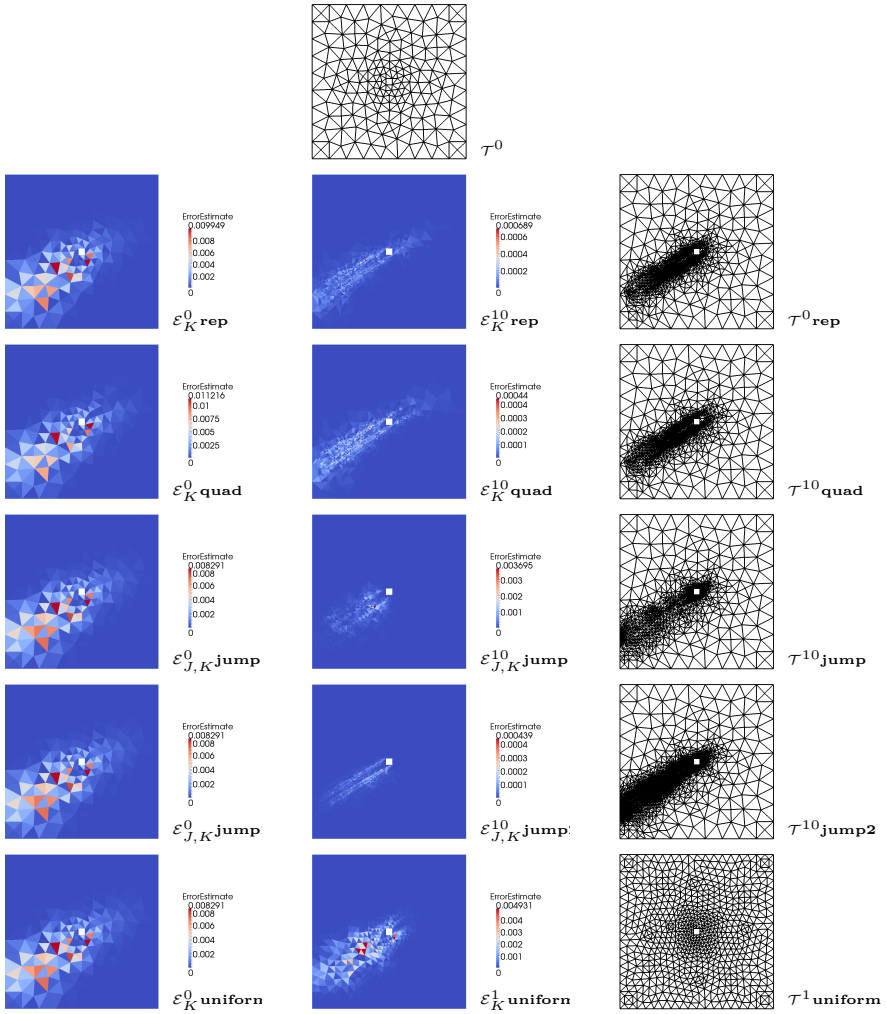

FIG. 6.9. *Comparison of adaptive error control quantitites and meshes for all methods for* $\epsilon = 10^{-5}, |\beta| = 1.171$